EXPERIMENTAL INVESTIGATION OF THE BLADE TIP TIMING (BTT) UNCERTAINTIES

Zhicheng XIAO[1], Yiming MENG[1],
Hua OUYANG[1, 2]

[1] *Shanghai Jiao Tong University, 800 Dongchuan, Minhang, 200240 Shanghai, PR China*

[2] *Engineering Research Center of Gas Turbine and Civil Aero Engine, 1500 Cenglin, Pudong, Shanghai 200000, PR China*

SUMMARY

The uncertainties of blade tip displacement measurement using BTT are investigated through experiments. A novel test bench is established where the blade deformation can be measured simultaneously by laser displacement sensors and BTT, which enables the determination of the BTT measurement error. It is discovered that the rotational speed fluctuation is the primary factor that degrades the accuracy of BTT. The magnitude of error is dependent on the probe position and could be up to 0.5 mm even when the rotor is driven by a servo. Fortunately, it is also validated that using multiple keyphasors could effectively elevate the accuracy of BTT measurement.

INTRODUCTION

Rotating blades in turbomachinery are prone to deformation and vibration. Harmful vibrations may induce high-cycle fatigue, which eventually leads to failures. To ensure long-time reliability, accurate measurement of blade vibration is significant in the stage of R&D and during service life.

Blade tip timing (BTT) is a popular technology for rotating blade certification and monitoring. A common method is to measure the time of arrival (ToA) of each blade by several sensors installed on the casing and then to calculate the blade tip displacements. Compared with strain gauges, BTT enjoys the advantage of being contactless, capable of long-term online monitoring of all the blades, and easy to deploy [1-3]. However, BTT measurement suffers from a severe undersampling problem because only a few samples could be collected within each revolution. In order to extract useful vibrational information from the undersampled data, researchers have put great effort into the development of processing algorithms [4-9]. Acquiring accurate tip displacement samples is still a

prerequisite to reliable mode recognition, which underlines the need for a high displacement measurement accuracy. In practice, it is often assumed that the rotational speed of the rotor can be regarded as uniform [1, 10]. However, Diamond *et al*. [11] proved experimentally that such an assumption is not naturally valid. In fact, it could introduce considerable errors. Further, Zhou *et al*. [12] analyzed the uncertainties caused by random speed fluctuations with normal distribution and uniform distribution. Recently, scholars have proposed some methods to reduce the error from speed fluctuation. Zhang *et al*. [13] proposed a method utilizing multiple keyphasors. They derived the measurement equation for this method and verified the feasibility by simulations. Ren *et al*. [14] proposed an error correction BTT (EC-BTT) method based on the modelling of speed fluctuation with different patterns and reducing them respectively.

One main difficulty to determine the BTT's accuracy is obtaining the benchmark data. A representative approach [15, 16] is to use strain gauges. However, the conversion from strain to displacement relies on finite element models. Since modelling errors are inevitable, the deduced displacements cannot function as benchmarks. Hence, the strain gauge is essentially an indirect method and is only suitable for researches about frequency domain characteristics. To study the accuracy of BTT, direct displacement measurements are still necessary.

In this work, a calibration system based on a laser displacement sensor is designed to obtain the benchmarks. Based on this, we are able to quantify the measurement error of BTT. Additionally, a high-precision rotary encoder is used to determine the source of error. The performances of the basic once-per-revolution method and the multiple-keyphasor method are discussed.

TIP DISPLACEMENT MEASUREMENT USING BTT

Basic model

Consider a set of BTT probes installed on a casing at the same axial position. To describe the motion of blades, two polar coordinate systems can be built. One is fixed on the casing, the other one is fixed on the rotor. Suppose that the axial and radial movements of the rotor are neglectable. Meanwhile, the rotor disk is assumed rigid because its deformation is trivial compared to the blades. Thus, the origins of the two reference frames should coincide on the rotational axis of the rotor. Figure 1 is a sketch of the described system.

The circumferential coordinates in the two frames satisfy the following transformation:

$$\theta^{\mathrm{C}} = \theta^{\mathrm{R}} + \varphi(t), \tag{1}$$

where the superscripts "C" and "R" stand for the casing and rotor frames, respectively. The angular displacement of the rotor disk is represented by $\varphi(t)$. Suppose the i-th blade triggers the j-th BTT probe at time t_{nij} in the n-th revolution, then the actual coordinate of the blade tip can be acquired by

$$\theta^{\mathrm{C}}_{\mathrm{blade},\,i} = \theta^{\mathrm{C}}_{\mathrm{probe},\,j} + 2\pi(n - 1),\ n = 1, 2, 3,\ldots \tag{2}$$

since the installation angle of probe $\theta^{\mathrm{C}}_{\mathrm{probe},\,j}$ is generally known. On the other hand, consider an undeformable blade, its ideal position at t_{nij} is

$$\bar{\theta}^{\mathrm{C}}_{\mathrm{blade},\,i} = \bar{\theta}^{\mathrm{R}}_{\mathrm{blade},\,i} + \varphi(t_{nij}). \tag{3}$$

Usually, the design position of blade $\bar{\theta}^{\mathrm{R}}_{\mathrm{blade},\,i}$ in Eq. (3) and the tip radius r are known variables. Therefore, the tip displacement can be obtained by

$$x_{nij} = r\,(\theta^{\mathrm{C}}_{\mathrm{blade},\,i} - \bar{\theta}^{\mathrm{C}}_{\mathrm{blade},\,i}) = r\,(\theta^{\mathrm{C}}_{\mathrm{probe},\,j} + 2\pi(n - 1) - \bar{\theta}^{\mathrm{R}}_{\mathrm{blade},\,i} - \varphi(t_{nij})). \tag{4}$$

Equation (4) implies that BTT measurement relies on the modelling of $\varphi(t)$. This is usually accomplished by a keyphasor sensor, or the OPR (once per revolution) sensor in some literature. A simple but very common model utilizes only one keyphasor and assumes that the disk keeps rotating at a uniform speed during the time interval between two consecutive triggers. For simplicity, we name this basic model the Piecewise Uniform speed Model with Single keyphasor (PUM-S). Mathematically, the PUM-S expresses the disk's angular displacement as

$$\varphi(t_{nij}) = \frac{t_{nij} - t_{\mathrm{key},\,n}}{t_{\mathrm{key},\,n+1} - t_{\mathrm{key},\,n}} + 2\pi(n - 1), \tag{5}$$

where $t_{\mathrm{key},\,n}$ is the instant when the keyphasor sensor is triggered in the beginning of the n-th revolution.

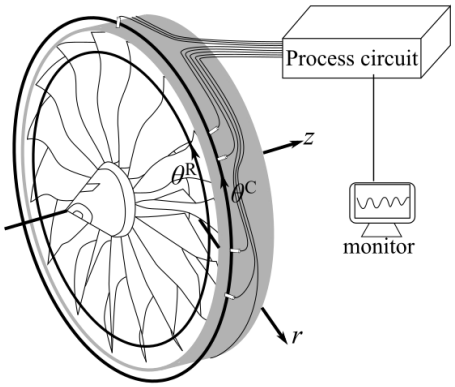

Figure 1: Sketch of the sensor installation and the coordinate system

Error analysis

During operations, the loads on the rotor blades are essentially unsteady. Consequently, the real rotational speed of the disk is hardly uniform. A strict description of the speed is

$$\varphi(t) = 2\pi(n - 1) + \int_{t_{\mathrm{key},\,n}}^{t} \omega(t)\,\mathrm{d}t\,,\ t_{\mathrm{key},\,n} \le t < t_{\mathrm{key},\,n+1}. \tag{6}$$

Define period $T_n = t_{\mathrm{key},\,n+1} - t_{\mathrm{key},\,n}$, nondimensionalized time $\tau = (t - t_{\mathrm{key},\,n}) / T_n$. Equation (6) can be rewritten as

$$\varphi(\tau) = 2\pi(n - 1) + T_n \int_0^{\tau} \omega(\tau)\,\mathrm{d}\tau\,,\ 0 \le \tau < 1. \tag{7}$$

The rotational speed can be decomposed using the Fourier series:

$$\omega = \bar{\omega}_n + \sum_{k=1}^{\infty} a_k \sin \pi k\tau + \sum_{k=1}^{\infty} b_k \cos \pi k\tau\,, \tag{8}$$

where the average speed $\bar{\omega}_n = 2\pi / T_n$. Generally, low frequency components account for a relatively large proportion in mechanical systems. Thus, the magnitude of a_k and b_k tend to decrease as k increases. Using Eq. (7) and (8),

$$\varphi(\tau) = 2\pi(n - 1) + T_n \left(\bar{\omega}_n \tau - \sum_{k=1}^{\infty} \frac{a_k}{\pi k} \cos \pi k\tau + \sum_{k=1}^{\infty} \frac{b_k}{\pi k} \sin \pi k\tau \right) + c. \tag{9}$$

We can define the uniform speed term $\bar{\varphi}(\tau) = T_n \bar{\omega}_n \tau = 2\pi\tau$ and the fluctuating term

$$\tilde{\varphi}(\tau) = T_n\left(\sum_{k=1}^{\infty}\frac{b_k}{\pi k}\sin\pi k\tau - \sum_{k=1}^{\infty}\frac{a_k}{\pi k}\cos\pi k\tau\right) + c. \tag{10}$$

The coefficients in Eq. (10) indicates that low frequency fluctuations of the rotational speed which correspond to small k may have considerable contributions to $\tilde{\varphi}(\tau)$, which would degrade the performance of the PUM-S model.

PUM with multiple keyphasors

A practical means to elevate the accuracy of the piecewise uniform speed model is utilizing multiple keyphasors (PUM-M). The principle can be explained through Taylor expansion

$$\varphi(\tau) = 2\pi(n - 1) + \varphi'(0)\tau + o(\tau^2). \tag{11}$$

PUM neglects the terms with order larger than 1. Therefore, shrinking τ could effectively reduce the truncation error.

From an engineering perspective, multiple keyphasors are easy to implement as long as single keyphasor has been established. Given the angular of position of m keyphasors $\theta^{\mathrm{R}}_{\mathrm{key},\,m}$, the PUM-M can be expressed as

$$\varphi(t_{nij}) = \frac{t_{nij} - t_{\mathrm{key},\,n,\,m}}{t_{\mathrm{key},\,n,\,m+1} - t_{\mathrm{key},\,n,\,m}}(\theta^{\mathrm{R}}_{\mathrm{key},\,m+1} - \theta^{\mathrm{R}}_{\mathrm{key},\,m}) + \theta^{\mathrm{R}}_{\mathrm{key},\,m} + 2\pi(n - 1). \tag{12}$$

EXPERIMENTAL METHOD

A high-accuracy test bench is built to determine the BTT measurement error as well as the source of it. Figure 2 shows the system configuration. Straight plate blades are adopted to simplify the rig design and manufacture. The tip radius for each blade is 270 mm. The blades are designed to be thin enough that obvious vibration can be created by merely the unsteady aerodynamic loads. Laser displacement sensors (LDS) are used to directly measure the blade tip displacement during operations, which is the most prominent feature of this bench. A slip-ring is used to transfer the signal from the rotating LDS to the stationary environment. The shaft is connected to a rotary encoder, which produces 10000 pulses in a single revolution. Hence, the rotational speed fluctuation can be captured with enough precision.

Limited by the power of the motor, the maximum speed in the experiments is 1200 rpm. Nevertheless, the results are found representative enough. Optical BTT sensors are distributed at random angles around the blades. To synchronize the data from BTT, LDS, and the encoder, a single collection system is used. The clock frequency of the system is 50 MHz, which is accurate enough for the experiments presented here.

RESULT AND DISCUSSION

BTT measurement error

Firstly, the raw measured data is studied in the time domain. Figure 3 compares the performance of BTT and LDS. Here, the basic PUM-S technique is adopted and the rotational speed is the averaged speed in each revolution. In Fig. 3, the displacement is set as 0 when the blade is at its balance position at 1500 rpm. Because the blades are designed to be thin and flat, they will suffer great drag force during rotation and bend notably. Accordingly, the data from LDS slowly drops to zero during acceleration. However, the BTT underestimates the displacement. This is due to the poor modelling of the angular movement of the disk. Using Eq. (11) to explain, the value of $\varphi'(0)$ is overestimated, and the residue terms are inappropriately ignored, causing the estimated $\varphi(\tau)$ greater than the true value. Then from Eq. (4), the calculated displacement x_{nij} will be smaller than the truth.

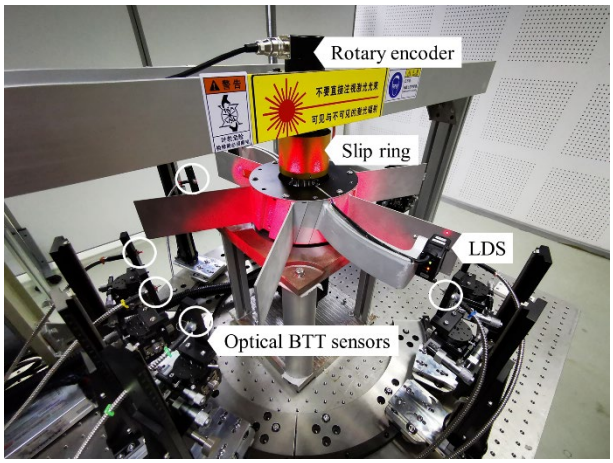

Figure 2: Test bench setup

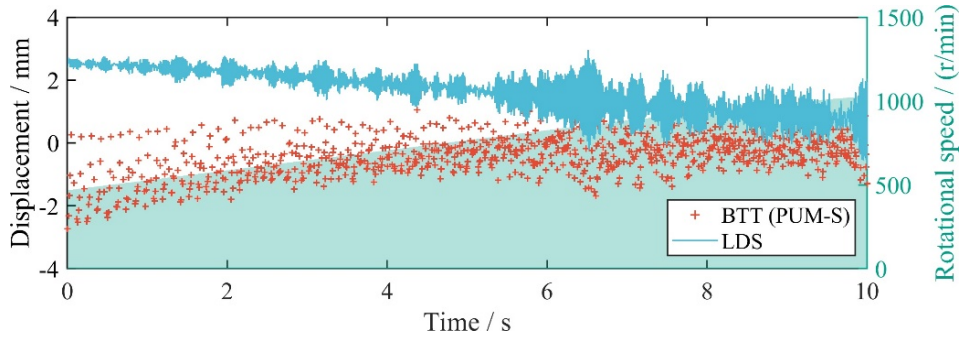

(a) Acceleration

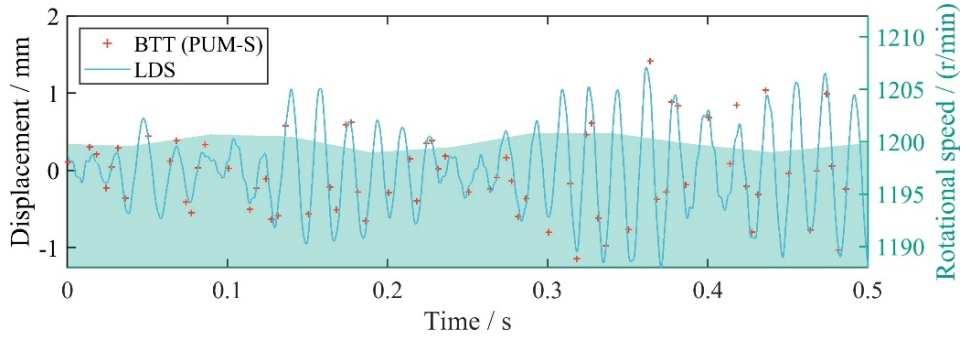

(b) Stable operation

Figure 3: Displacement measured by BTT and LDS

At a stable operational condition, the results of the two systems become close. Yet, not all the BTT samples coincide with the LDS plot. Additionally, the rotational speed exhibited in Fig. 3(b) is clearly fluctuating.

To quantify the accuracy of BTT probes, two statistical indicators are studied. One is the correlation between BTT and LDS, the other one is the standard deviation of BTT errors. The results are plotted in Fig. 4. The scatters represent the measured data and the dashed lines show the fittings. Both the correlation and the deviation exhibit trends related to the rotational speed. The correlation is merely 0.2-0.8 at 300 rpm while it soars to more than 0.9 at 900 rpm. However, no obvious elevation can be observed when the speed further increases to 1200 rpm.

Although the correlation at 300 rpm is low, the standard deviation is the smallest among the four cases. As the rotational speed grows, the deviation increases monotonously. Meanwhile, the distribution of the data is symmetric to the key-phase sensor. The opposite position to the key-phase sensor witnesses the maximum 3σ of more than 0.5 mm. Considering that a servo is used in our facility, the situation faced by an industrial rig could possibly be worse.

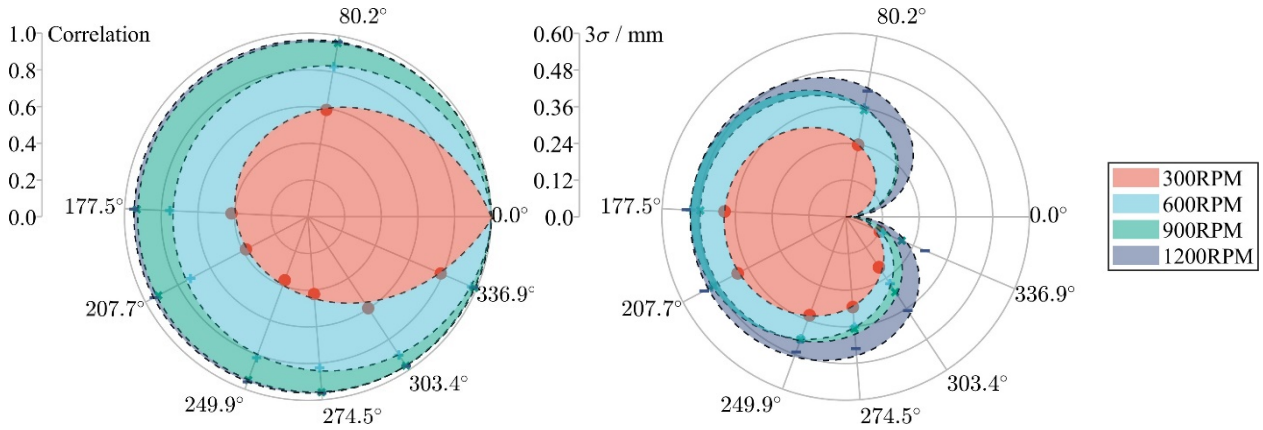

(a) Correlation coefficient between BTT and LDS *(b) Standard deviation of BTT error*

Figure 4: Statistical performance of BTT sensors at different angles

Error source identification

The most possible explanation for all the phenomena listed in the previous section is that the main source of error is speed fluctuation. At low speeds, the error and the truth share similar but small magnitudes, leading to a small deviation but also a low correlation. As the speed increases, both the displacement and the error increase, while the proportion of error in the displacement decreases. The correlation finally reaches an upper limit less than unit because of the existence of speed fluctuation error.

To validate the explanation, the data from the rotary encoder is utilized. Figure 5 plots the error of $\varphi(t)$ estimation by PUM-S. In Fig. 5(a), the error displays a quasi-periodic pattern during acceleration. By contrast, the error is more of a random variable during stable operations in Fig. 5(b). The magnitude of the $\varphi(t)$ estimation error is just the same as the total error of BTT, e_{total}. To further demonstrate their relationship, we extracted the estimation error e_{φ} at the BTT sampling instants and plot it against e_{total} as shown in Fig. 6. The scatter points display a typical proportional relationship. Therefore, we can prove that the main factor of contaminating BTT measurements is the speed fluctuation error.

Elevating accuracy using multiple key-phases

The capability of PUM-M to suppress the speed fluctuation error is studied. First, to corrected apply the PUM-M, the exact position of each keyphasor must be carefully calibrated. This is accomplished by taking the averages during stable operational conditions:

$$\theta^{\text{R}}_{\text{key},\,m} = \frac{2\pi}{N}\sum_{n=1}^{N}\frac{t_{\text{key},\,n,\,m} - t_{\text{key},\,n,\,1}}{t_{\text{key},\,n+1,\,1} - t_{\text{key},\,n,\,1}}. \tag{13}$$

Despite that we design the key-phases to distribute uniformly around the circumference, tiny offset is unavoidable:

$$\delta_m = \theta^{\text{R}}_{\text{key},\,m} - \frac{m}{M} \tag{14}$$

where M is the total number of keyphasors. Figure 7 shows the convergence history of one key-phase position. The offset δ_m quickly converges to a narrowband as the number of revolution N increases. It eventually stabilizes in a small interval of 0.004 mm, which is accurate enough compared to the BTT error.

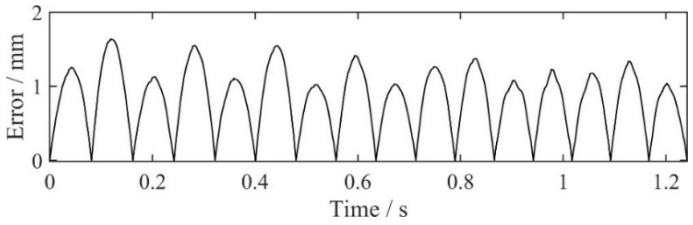

(a) A segment during acceleration

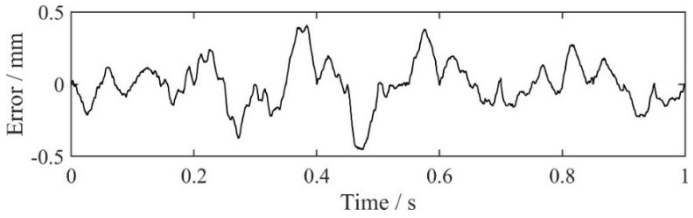

(b) Stable operation

Figure 5: Error of $\varphi(t)$ estimation by PUM-S

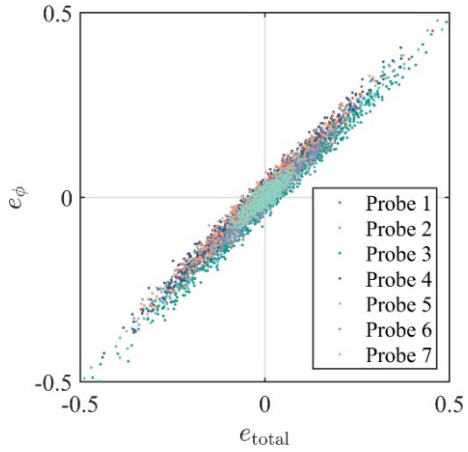

Figure 6: Relationship between e_{total} and e_φ

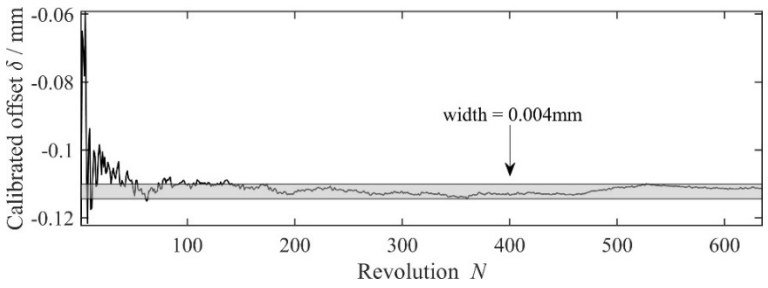

Figure 7: Convergence of the keyphasor calibration

Using the calibrated keyphasor positions, PUM-M can now work as expected. Figure 8 depicts the displacement calculated by PUM-M using the same dataset as in Fig. 3. Almost all the BTT samples coincide with the LDS result. Figure 9 plots the relationships between the number of keyphasors and the BTT error. More than 50 % of the error could be removed for probes 2 and 3. These are the two sensors farthest from the original keyphasor. The reduction of their errors could significantly improve the accuracy of whole circumferential data analysis. It is worth mentioning that in the experiment, the errors of all probes converge to 80 μm. However, they are supposed to decrease to 0 as the number of keyphasors increases. The discrepancy between the theory and the practice comes from the defects in the mechanical structural. Due to the poor machining accuracy, the upper and lower pivot of the rotor are not well aligned. A flexible coupling is applied to connect the rotor shaft and the rotary encoder in order to alleviate the vibration at high speeds. Consequently, slight relative motion between the encoder and the shaft could take place, leading to the tiny difference

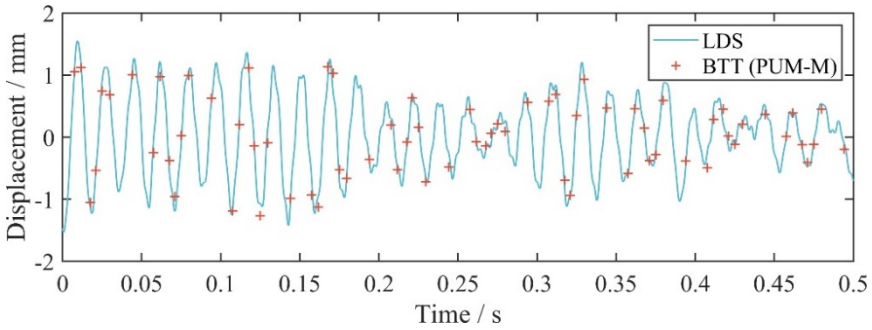

Figure 8: Displacement measurement using BTT (PUM-M) and LDS

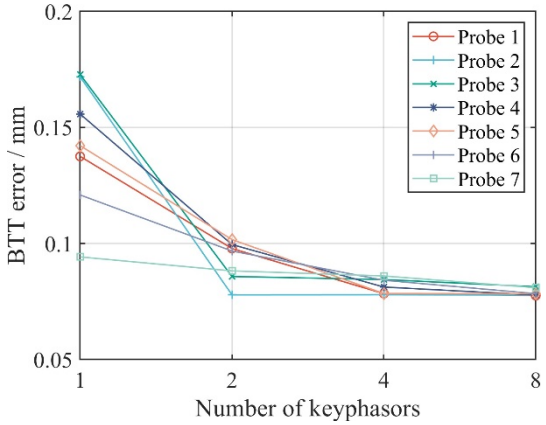

Figure 9: Descend of error with multiple keyphasors

between the ideal signal and the measured signal from the encoder. Nevertheless, an accuracy of 80 μm is well enough in industrial applications.

CONCLUSIONS

In this paper, a new test bench is designed to obtain the benchmark data of blade tip displacement. Based on this, the measurement error of BTT is studied. The conclusions are summarized as follows.

First, when the basic PUM-S method is adopted, the speed fluctuation error is the main contributor to the total error of BTT.

Second, the error varies among different BTT probes and exhibits a symmetric distribution to the key-phase sensor. On the opposite position, the standard deviation reaches its maximum. The 3σ is up to 0.5 mm. Considering that a servo is used in this work, the situation faced by an industrial rig could possibly be worse.

Third, the application of PUM-M could effectively reduce the speed fluctuation error as long as the keyphasor positions are correctly calibrated. The standard error could drop to less than 0.1 mm when 8 keyphasors are used. Therefore, it is strongly recommended to use multiple key-phases when there is a high demand for measurement accuracy.

ACKNOWLEDGEMENTS

This work is supported by the National Science and Technology Major Project under Grant 2017-II-0007-0021 and J2019-II-0005-0025. The authors would like to acknowledge Li Jianping and Zhang Yin for their contributions to the experiments.

BIBLIOGRAPHY

[1] Z. Chen, H. Sheng, Y. Xia, W. Wang, J. He - *A comprehensive review on blade tip timing-based health monitoring: status and future*. Mechanical Systems and Signal Processing, 149: 107330, **2021**

[2] R. Przysowa, P. Russhard - *Non-contact measurement of blade vibration in an axial compressor*. Sensors, 20(1): 68, **2020**

[3] P. Russhard - *The rise and fall of the rotor blade strain gauge*. Vibration Engineering and Technology of Machinery, Springer, Switzerland, pp. 27-37, **2015**

[4] I.Y. Zablotskiy, Y.A. Korostelev - *Measurement of resonance vibrations of turbine blades with the Elura device*, Energomashinostroneniye 36-39, **1970**.

[5] S. Heath - *A new technique for identifying synchronous resonances using tip-timing*, International Gas Turbine & Aeroengine Congress & Exhibition, 99-GT-402, **1999**.

[6] I. B. Carrington, J. R. Wright, J. E. Cooper, G. Dimitriadis - *A comparison of blade tip timing data analysis methods*, Proceedings of the Institution of Mechanical Engineers, Part G: Journal of Aerospace Engineering 215(5) 301–312, **2001**.

[7] H.T. Corporation, *Overview of blade vibration monitoring capabilities*, **2011**.

[8] V. Kharyton, G. Dimitriadis, C. Defise - *A discussion on the advancement of blade tip timing data processing*, ASME Turbo Expo, GT2017-63138, **2017**.

[9] Z. Zhang, P. Chai, Y. Chen, J. Tian, H. Ouyang - *Optimization of non-uniform sensor placement for blade tip timing based on equiangular tight frame theory*, Journal of Engineering for Gas Turbines and Power, GTP-21-1304, **2021**.

[10] P. Russhard - *Blade tip timing (BTT) uncertainties*, 12th International A.I.VE.LA. Conference on Vibration Measurements by Laser and Noncontact Techniques, AIP, 020003, **2016**.

[11] D.H. Diamond, P.S. Heyns, A.J. Oberholster, *Online shaft encoder geometry compensation for arbitrary shaft speed profiles using Bayesian regression*, Mechanical Systems and Signal Processing 81, 402-418, **2016**.

[12] C. Zhou, H. Hu, F. Guan, Y. Yang, *Modelling and simulation of blade tip timing uncertainty from rotational speed fluctuation*, Prognostics and System Health Management Conference, pp. 1-5, **2017**.

[13] Z. Ji-wang, Z. Lai-bin, D. Ke-Qin, D. Li-xiang - *Blade tip-timing technology with multiple reference phases for online monitoring of high-speed blades under variable-speed operation*, Measurement Science Review 18(6) 243-250, **2018**.

[14] S. Ren, X. Xiang, W. Zhao, Q. Zhao, C. Wang, Q. Xu - *An error correction blade tip-timing method to improve the measured accuracy of blade vibration displacement during unstable rotation speed*, Mechanical Systems and Signal Processing 162, 108030, **2022**.

[15] M. E. Mohamed - *Towards reliable and efficient calibration of blade tip timing measurements against finite element model predictions*, Department of Mechanical, Aerospace, and Civil Engineering, University of Manchester, **2019**.

[16] G. Battiato, C.M. Firrone, T.M. Berruti, *Forced response of rotating bladed disks: Blade tip-timing measurements*, Mechanical Systems and Signal Processing 85, 912-926. **2017**.